Modeling and minimizing interference from corneal birefringence in retinal birefringence scanning for foveal fixation detection

Kristina Irsch,* Boris Gramatikov, Yi-Kai Wu, and David Guyton

The Wilmer Ophthalmological Institute, The Johns Hopkins University School of Medicine, Wilmer 233, The Johns Hopkins Hospital, 600 N. Wolfe Street, Baltimore, MD 21287-9028, USA
**kirsch1@jhmi.edu*

Abstract: Utilizing the measured corneal birefringence from a data set of 150 eyes of 75 human subjects, an algorithm and related computer program, based on Müller-Stokes matrix calculus, were developed in MATLAB for assessing the influence of corneal birefringence on retinal birefringence scanning (RBS) and for converging upon an optical/mechanical design using wave plates ("wave-plate-enhanced RBS") that allows foveal fixation detection essentially independently of corneal birefringence. The RBS computer model, and in particular the optimization algorithm, were verified with experimental human data using an available monocular RBS-based eye fixation monitor. Fixation detection using wave-plate-enhanced RBS is adaptable to less cooperative subjects, including young children at risk for developing amblyopia.

OCIS codes: (170.4460) Ophthalmic optics and devices; (170.4470) Ophthalmology; (260.1440) Birefringence; (260.5430) Polarization; (330.4300) Vision system - noninvasive assessment; (330.7326) Visual optics, modeling

References and links

1. D. L. Guyton, D. G. Hunter, S. N. Patel, J. C. Sandruck, and R. L. Fry, "Eye fixation monitor and tracker," U.S. Patent No. 6,027,216 (Feb. 22, 2000).
2. D. G. Hunter, S. N. Patel, and D. L. Guyton, "Automated detection of foveal fixation by use of retinal birefringence scanning," Appl. Opt. **38**(7), 1273–1279 (1999).
3. L. R. Young and D. Sheena, "Survey of eye movement recording methods," Behav. Res. Meth. Instrum. **7**(5), 397–429 (1975).
4. D. G. Hunter, A. S. Shah, S. Sau, D. Nassif, and D. L. Guyton, "Automated detection of ocular alignment with binocular retinal birefringence scanning," Appl. Opt. **42**(16), 3047–3053 (2003).
5. D. G. Hunter, D. S. Nassif, N. V. Piskun, R. Winsor, B. I. Gramatikov, and D. L. Guyton, "Pediatric Vision Screener 1: instrument design and operation," J. Biomed. Opt. **9**(6), 1363–1368 (2004).
6. K. Irsch, "Polarization modulation using wave plates to enhance foveal fixation detection in retinal birefringence scanning for pediatric vision screening purposes," Ph.D. thesis (University of Heidelberg, Germany, 2009), http://www.ub.uni-heidelberg.de/archiv/8938/.
7. B. I. Gramatikov, O. H. Y. Zalloum, Y. K. Wu, D. G. Hunter, and D. L. Guyton, "Birefringence-based eye fixation monitor with no moving parts," J. Biomed. Opt. **11**(3), 034025 (2006).
8. D. S. Nassif, N. V. Piskun, B. I. Gramatikov, D. L. Guyton, and D. G. Hunter, "Pediatric Vision Screener 2: pilot study in adults," J. Biomed. Opt. **9**(6), 1369–1374 (2004).
9. D. S. Nassif, N. V. Piskun, and D. G. Hunter, "The Pediatric Vision Screener III: detection of strabismus in children," Arch. Ophthalmol. **124**(4), 509–513 (2006).
10. R. W. Knighton and X. R. Huang, "Linear birefringence of the central human cornea," Invest. Ophthalmol. Vis. Sci. **43**(1), 82–86 (2002).
11. R. N. Weinreb, C. Bowd, D. S. Greenfield, and L. M. Zangwill, "Measurement of the magnitude and axis of corneal polarization with scanning laser polarimetry," Arch. Ophthalmol. **120**(7), 901–906 (2002).
12. A. W. Dreher and K. Reiter, "Retinal eye disease diagnostic system," U.S. Patent No. 5,303,709 (Apr. 19, 1994).
13. B. C. E. Pelz, C. Weschenmoser, S. Goelz, J. P. Fischer, R. O. W. Burk, and J. F. Bille, "In vivo measurement of the retinal birefringence with regard on corneal effects using an electro-optical ellipsometer," Proc. SPIE **2930**, 92–101 (1996).
14. Q. Zhou and R. N. Weinreb, "Individualized compensation of anterior segment birefringence during scanning laser polarimetry," Invest. Ophthalmol. Vis. Sci. **43**(7), 2221–2228 (2002).
15. Q. Zhou, "System and method for determining birefringence of anterior segment of the patient's eye," U.S. Patent No. 6,356,036 (March 12, 2002).

#146653 - $15.00 USD Received 2 May 2011; revised 15 Jun 2011; accepted 15 Jun 2011; published 17 Jun 2011

16. R. W. Knighton and X. R. Huang, "Analytical methods for scanning laser polarimetry," Opt. Express **10**(21), 1179–1189 (2002).
17. Q. Zhou, "Retinal scanning laser polarimetry and methods to compensate for corneal birefringence," Bull. Soc. Belge Ophtalmol. **302**(302), 89–106 (2006).
18. N. J. Reus, Q. Zhou, and H. G. Lemij, "Enhanced imaging algorithm for scanning laser polarimetry with variable corneal compensation," Invest. Ophthalmol. Vis. Sci. **47**(9), 3870–3877 (2006).
19. D. G. Hunter, J. C. Sandruck, S. Sau, S. N. Patel, and D. L. Guyton, "Mathematical modeling of retinal birefringence scanning," J. Opt. Soc. Am. A **16**(9), 2103–2111 (1999).
20. M. C. Müllenbroich, "Design and construction of a fixation stability monitor for diagnosis and management of ADHD," Master's thesis (University of Heidelberg, Germany, 2006).
21. F. A. Bettelheim, "On the optical anisotropy of lens fiber cells," Exp. Eye Res. **21**(3), 231–234 (1975).
22. R. A. Weale, "Sex, age and the birefringence of the human crystalline lens," Exp. Eye Res. **29**(4), 449–461 (1979).
23. H. B. klein Brink, "Birefringence of the human crystalline lens in vivo," J. Opt. Soc. Am. A **8**(11), 1788–1793 (1991).
24. G. J. Van Blokland and S. C. Verhelst, "Corneal polarization in the living human eye explained with a biaxial model," J. Opt. Soc. Am. A **4**(1), 82–90 (1987).
25. R. W. Knighton, X. R. Huang, and L. A. Cavuoto, "Corneal birefringence mapped by scanning laser polarimetry," Opt. Express **16**(18), 13738–13751 (2008).
26. H. B. klein Brink and G. J. van Blokland, "Birefringence of the human foveal area assessed in vivo with Mueller-matrix ellipsometry," J. Opt. Soc. Am. A **5**(1), 49–57 (1988).
27. G. J. van Blokland, "Ellipsometry of the human retina in vivo: preservation of polarization," J. Opt. Soc. Am. A **2**(1), 72–75 (1985).
28. S. N. Patel, "Analysis of foveal birefringence to monitor eye fixation," Master's thesis (Johns Hopkins University, Baltimore, MD, 1995).
29. A. W. Dreher, K. Reiter, and R. N. Weinreb, "Spatially resolved birefringence of the retinal nerve fiber layer assessed with a retinal laser ellipsometer," Appl. Opt. **31**(19), 3730–3735 (1992).
30. R. W. Knighton, "Spectral dependence of corneal birefringence at visible wavelengths," Invest. Ophthalmol. Vis. Sci. 43, E-Abstract 152 (2002).
31. E. Collet, *Polarized Light, Fundamentals and Applications* (Marcel Dekker, New York, 1993).
32. K. Irsch, B. I. Gramatikov, Y. K. Wu, and D. L. Guyton, "Spinning wave plate design for retinal birefringence scanning," Proc. SPIE **7169**, 71691F (2009).

1. Introduction

Retinal birefringence scanning (RBS) is a technique to monitor the changes in the state of polarized light retro-reflected from the fundus of the human eye. It was adapted by Guyton and colleagues to detect foveal fixation [1,2]. For fixation detection using RBS, polarized near-infrared light is directed onto the retina in a circular scan (subtending 3° of visual angle), with a fixation point in the center, and the polarization-related changes in light retro-reflected from the ocular fundus are analyzed by means of differential polarization detection. Due to the radially symmetric arrangement of the birefringent Henle fibers about the fovea, a characteristic frequency that is a multiple of the scanning frequency appears in the obtained periodic signal, for example twice the scanning frequency ($2f$) when the scan is exactly centered on the fovea, as described in detail previously [1,2], which is the case with central fixation. Thus, by analyzing the generated frequencies in the obtained RBS signal, the goodness of eye fixation can be measured.

The main advantage of RBS-based detection of eye fixation over other methods [3], such as scleral search coils, electro-oculography, and video-based eye trackers, is that it does not require eye-gaze calibration. By detecting the radial symmetry of the foveal architecture, RBS directly assesses true foveal fixation of the eye. This advantage makes it possible to investigate less cooperative subjects, including young children and infants at risk for developing amblyopia, commonly known as "lazy eye," which is the leading medical cause of decreased vision in childhood. Binocular RBS has the potential for automatic and reliable screening of infants and young children for misalignment of the eyes (strabismus) [4–6], the most common cause of amblyopia. Currently available photoscreeners can only detect strabismus indirectly and inaccurately via assessment of the positions of the corneal light reflexes.

Previous generations of our so-called RBS-based eye fixation monitor demonstrated reliable, non-invasive detection of foveal fixation [2,7], as well as detection of strabismus [4,5,8,9]. However, as with all polarization-sensitive technology used for retina assessment,

#146653 - $15.00 USD Received 2 May 2011; revised 15 Jun 2011; accepted 15 Jun 2011; published 17 Jun 2011

RBS is adversely affected by the corneal birefringence, whose variation from one eye to the next caused significant variability of previous RBS signal levels among individuals. Although being relatively constant over the entrance pupil of any given eye, corneal birefringence, which contributes most (~50-90%) to the overall ocular birefringence, varies widely in both its amount (corneal retardance) and orientation (corneal azimuth) from one eye to the next [10,11]. That variability is substantial enough to produce large, uncontrolled differences in the amplitudes of the detected signals in retro-reflective birefringence scanning, and these changes can mask the desired polarization-related changes induced by the retina.

Various methods have been proposed in the literature to factor out or compensate for corneal birefringence [12–18], but all involve a separate measurement and feedback system, an approach that is tedious and not feasible in poorly cooperative children. Also, most applications of retinal birefringence scanning have required stabilization of the subject's head to enable alignment of the instrument's tiny exit pupil (<2 mm) within the subject's pupil.

When testing unrestrained young children, we must use a hand-held instrument with large exit pupils (about 40 x 40 mm for each eye) that can be aimed at the child's eye(s). With varying gaze directions, though, corneal birefringence can vary continuously during a recording with a moving child, so that a method of bypassing rather than compensating for the corneal birefringence is desired, especially in an application that is geared towards children. The most promising approach involves the application of wave plates because of their ability to influence the polarization state of light. When properly applied, they can shift the detected polarization states into ranges that are minimally affected by different amounts and orientations of corneal birefringence.

To achieve a better understanding of the influence of corneal birefringence on the detected RBS signals, we developed a computer model in MATLAB, based on a previously developed mathematical model from our lab [19], simulating retinal birefringence scanning in a double-pass system using Müller-Stokes matrix calculus. Using this computer model, different options for the RBS design could be simulated to allow us to converge on an optical/mechanical design which optimally bypasses corneal birefringence and thus allows foveal fixation detection essentially independently of the various amounts and orientations of corneal birefringence that occur in the population. Our RBS computer model was validated experimentally using an available monocular RBS-based eye fixation monitor [20].

While the previously developed mathematical model, from which the current computer model described in this article was developed, has been shown to predict accurately the frequency and phase of the RBS signal during central and paracentral fixation [19], the effect of varying corneal birefringence on the strength of the RBS signals has not yet been considered, or verified with actual eyes. Thus, we wished to verify the ability of our RBS computer model to assess the variation in RBS signals with different amounts and orientations of corneal birefringence that occur in the population. We wished especially to test the model's ability to guide us to a design using wave plates ("wave-plate-enhanced RBS") that improves RBS signal strength across the population range of corneal retardances and azimuths.

2. Methods

2.1. Computer modeling of retinal birefringence scanning

Each optical component of the eye is characterized by its own Müller matrix (**M**), with the cornea and retina considered simply as birefringent media that affect the polarization state of transmitted light. Because the birefringence contribution of the crystalline lens is negligible [21–23], it is not included in the model. The double pass into and back out of the eye can thus be described mathematically by multiplying the Stokes vector ($\vec{S}_{in}$), defining the polarization state of the incident light, by the respective Müller matrices for each contributing ocular medium in sequence, i.e. the cornea, retina, reflection from the ocular fundus, retina again, and cornea again. The outgoing Stokes vector, $\vec{S}_{out}$, determines the final polarization state.

#146653 - $15.00 USD Received 2 May 2011; revised 15 Jun 2011; accepted 15 Jun 2011; published 17 Jun 2011

$$\vec{S}_{out} = \mathbf{M}_{cornea(out)}(CR,-CA)\cdot\mathbf{M}_{retina(out)}(\delta_{r,}-\theta_r)\cdot\mathbf{M}_{fundus} \cdot\mathbf{M}_{retina(in)}(\delta_{r,}\theta_r)\cdot\mathbf{M}_{cornea(in)}(CR,CA)\cdot\vec{S}_{in}. \quad (1)$$

The differential polarization signal measured by a polarizing beam splitter and a pair of photodetectors can be considered identical to the measurement of the S_1 component of the returning light, which represents Stokes parameter S_1.

The cornea is modeled as a linear retarder, specified by a certain retardance (CR) and azimuth (CA). The latter is simply the orientation of the fast axis of the retarder. In general, most corneas should be treated as a curved biaxial crystal with one optic axis perpendicular to the corneal surface and another optic axis parallel to the corneal surface [24,25]. For a light beam approximately perpendicular to the corneal surface, however, the cornea can be approximated as a linear retarder with a fixed retardance [10,25].

The Henle fiber layer is modeled as a radially birefringent medium, with every fiber acting as a linear retarder. Each fiber of the radially arrayed Henle fiber layer is assumed to have the same amount of birefringence (δ_r) with its slow axis aligned with the orientation of the fiber. The azimuth of the fast axis (θ_r), therefore, is perpendicular to the orientation of the fiber. As polarized light is scanned around the fovea in an annular pattern, the azimuth of the foveal birefringence depends on the orientation of the fibers at the current scanning position. During simulated central fixation, fiber orientation and scanning angle are identical, thus the azimuth of foveal birefringence is rotating through 360°. During paracentral fixation, however, the orientation of the fibers encountered at the momentary scanning position is a function of the point of fixation, so that the fast axis of foveal birefringence, being perpendicular to the fiber orientation, can be calculated as follows:

$$\theta_r = \tan^{-1}\left(\frac{R\sin(\varphi)+y_{ret}}{R\cos(\varphi)+x_{ret}}\right)+90° \quad (2)$$

where φ is the momentary scanning position, advancing through 360°, and x_{ret} and y_{ret} are the horizontal and vertical displacements of the center of the scanning circle from the fovea respectively. The amount of retinal birefringence, i.e. retinal retardance (δ_r), on the other hand, depends on the distance from the foveal center. In the RBS computer model, the maximum retardance is considered to be 15 nm [26,27], increasing from zero in the very center to the maximum of 15 nm ~1.5° from the center, and then tapering off farther from the center. This attenuation away from the center is described by [7]:

$$\delta_r = \left(\prod_{i=1}^{2} e^{-\frac{r}{\tau_i}}\right)\left(\prod_{i=3}^{5}\left(1-e^{-\frac{r}{\tau_i}}\right)\right) \quad (3)$$

where $\tau_1 = 3.7$, $\tau_2 = 50$, $\tau_3 = 0.6$, $\tau_4 = 5$, $\tau_5 = 0.8$ [7,28].

With central fixation, the 3° annulus formed by the scanned light beam is centered on the radial array of linear retarders, so that the same amount of retinal birefringence, i.e. retinal retardance, is experienced at each scanning position. Thus, given that the eye is fixating properly, the circular scan on the retina can be thought of, and simulated as, a spinning wave plate with a retardance of 15 nm, rotating at the frequency of the scan. For an operating wavelength of 785 nm, as used in our applications, 15 nm corresponds to a retardance of about 7°.

Because reflection from the ocular fundus exhibits a high degree of polarization preservation [29], the fundus is treated as a complete polarization-preserving ideal reflector, modeled by the Müller matrix of an ideal mirror:

#146653 - $15.00 USD Received 2 May 2011; revised 15 Jun 2011; accepted 15 Jun 2011; published 17 Jun 2011

$$\mathbf{M}_{fundus} = \begin{pmatrix} 1 & 0 & 0 & 0 \\ 0 & 1 & 0 & 0 \\ 0 & 0 & -1 & 0 \\ 0 & 0 & 0 & -1 \end{pmatrix}. \quad (4)$$

As can be seen, the reflection from the fundus simply reverses the signs of Stokes parameters S_2 and S_3, while the sign of S_1 remains unchanged.

2.2. Assessing the influence of corneal birefringence on the RBS signal

Both corneal retardance and azimuth vary from one eye to the next but are reasonably constant over the entrance pupil for any given eye. To consider the different values for CR and CA that occur in the population, we used the 140 eyes (70 right eyes and 70 left eyes) from the data published by Knighton and Huang as a reference [10]. Within the scope of their studies, normal subjects were measured (at a wavelength of 585 nm) to determine the birefringence properties (slow axis and double-pass retardance) of their central corneas. Five additional pairs of CR and CA were included in the assessment, obtained from measurements (in the near infrared) in our laboratory [7]. As corneal birefringence is essentially constant across wavelengths [30], there should not be significant differences in corneal birefringence values between the two data sets. Since our RBS computer model expects single-pass corneal retardance and corneal fast axis (CA), the following calculations were performed to match the corneal parameters in the model: 1) corneal double-pass retardance values were converted to single-pass values; 2) corneal slow axis (CSA) values, measured nasally downward for each eye in the original data set [10], were converted to corneal fast axis (CA) values as follows:

$$\mathrm{CA} = \mathrm{CSA} + 90°, \quad (5)$$

where for the right eyes, CSA corresponds to the negative value of the measured corneal slow axis. This yielded a common azimuth scale for both eyes, ranging from 0° (subject's right ear) to 180° (subject's left ear), with a rough symmetry of right and left eye corneal azimuths about the nose (about CA = 90°). In fact, 99% of right eye corneal azimuths and 96% of left eye corneal azimuths in the data set are between 0° and 90°, and 90° and 180°, respectively. As corneal azimuths between the two eyes are well correlated, r = 0.77 [10], and approximately symmetrical about 90° CA (average meridian of symmetry between both eyes is 92.7° for the subjects in our data set), and because we wanted to derive a symmetric solution to simplify the mechanical construction of the apparatus (further explained below) covering a wide range of potential right and left eye corneal birefringences, we included the mirror image of each eye (mirrored about 90° CA) in the assessment, yielding a total number of 300 representative pairs of CR/CA. In the further course of this paper, the data representing these 300 "eyes" are referred to as the Knighton/Gramatikov data set. The data set contains values, however, from only 75 truly independent eyes plus 75 fellow eyes.

In addition to modeling the effects of ocular birefringence as described above, the RBS computer program provides the user with a means to select diverse optical components and to specify their properties in the double-pass scanning system. These manipulations can alter the polarization state of light in various ways before and after passing through the eye in order to optimize the power throughput and converge toward an RBS design that yields the largest differential RBS signal practically constant over the population range of corneal retardances and azimuths. For instance, additional wave plates can be optionally placed in the light path, single-pass or double-pass (operating in either the incoming path or in the return path, or in both), rotating or fixed, as well as beam splitters, etc. With the help of the Knighton/Gramatikov data set, it was possible to judge if a certain RBS design would fail or excel over a significant proportion of the population (further explained below).

For a given optical arrangement, the model retina is scanned in a circle with incident linearly vertical polarized light ($\vec{S}_{in}$ = $(1,-1,0,0)^T$) 16 times in total (as with our actual RBS-

#146653 - $15.00 USD Received 2 May 2011; revised 15 Jun 2011; accepted 15 Jun 2011; published 17 Jun 2011

based eye fixation monitors), in incremental steps of 4.5°, thus leading to 1280 "measurements." The resulting periodic RBS signal is Fourier analyzed to determine the predominant component frequencies. More precisely, the Fast Fourier Transform (FFT) is computed on the whole 16-cycle epoch, an epoch long enough to provide good frequency resolution, and the power spectrum values at the frequencies of interest are determined for a range of CR and CA combinations (0 nm to 180 nm CR, and 0° to 180° CA) to cover the variability of corneal birefringence across individuals. These signal strengths (FFT power) at a given frequency are displayed as a function of CR and CA over the entire ranges of these variables (Fig. 1(a)). Superimposed on the surface of this 3D-plot are the specific pairs of CR and CA of the Knighton/Gramatikov data set, so that it is readily visible how the optical arrangement would perform across a representative group of people. Right eyes (and mirrored left eyes) are indicated as circles and left eyes (and mirrored right eyes) as crosses. In the best case, the surface of the 3D-plot should be flat and high according to the requirements of greatest independence from corneal birefringence. The contour plot, which is generated simultaneously with the 3D-plot, provides another means of judgment about the suitability of a design. This contour plot is simply a flat graph with axes CA and CR, showing in the background the corneal retardance and azimuth of each of the "right" and "left" eyes in the Knighton/Gramatikov data set, upon which is superimposed a contour plot of the signal strength showing where the signal drops down, thereby indicating which eyes are missed when the signal falls below the threshold of 0.4, which has been arbitrarily considered as a measurement failure (Fig. 1(b)).

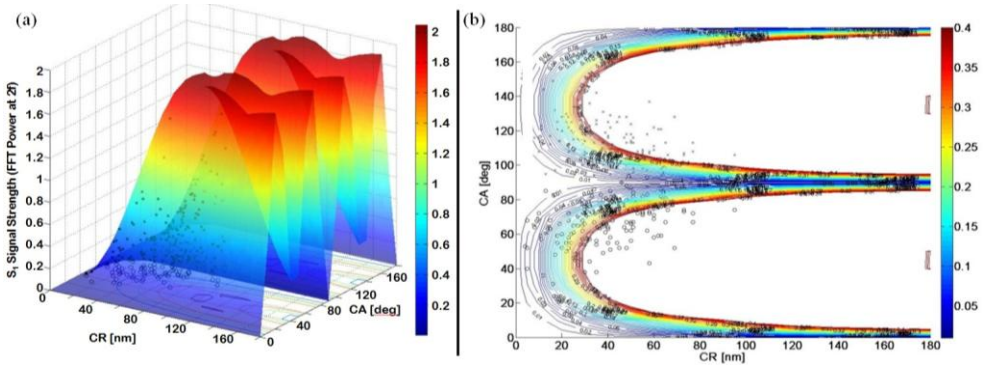

Fig. 1. (a) RBS signal strength at 2*f* (in relative power units) as a function of corneal retardance (CR) and corneal azimuth (CA) during simulated central fixation with computer model of the RBS design implemented into the eye fixation monitor used for model validation purposes (see Subsection 2.3). (b) Contour plot of (a), with contours plotted only up to a signal strength of 0.4. Eyes that fall within the white regions (where the signal is above the threshold of 0.4) will yield strong enough signals for reliable detection, and eyes in the colored regions will not. Please note the different scales on the color bar. Right eyes (and mirrored left eyes) are indicated as circles and left eyes (and mirrored right eyes) as crosses.

Figures 1(a) and 1(b) are the predicted results during simulated foveal fixation with the RBS-based eye fixation monitor used for the purpose of model validation (see 2.3). As can be seen, the RBS signal obtained with the current RBS design implemented into the eye fixation monitor is poor for eyes with very low corneal retardance and goes to zero when corneal retardance is zero. The design is more favorable for eyes with higher corneal retardances, including outliers with very high corneal retardances (up to 125 nm single-pass) excluded in [10]. Moreover, for either eye, the signal falls off with low or high corneal azimuth. More precisely, the signal goes to zero when corneal azimuth is 0°, 90°, and 180°. As shown in Fig. 1(b), 204 of the representative "eyes" (102 of either eye), from the Knighton/Gramatikov data set of 300 "eyes" fall below the "0.4" contour. In other words, with this threshold setting, 68% of the "eyes" in the data set fail with the RBS-based eye fixation monitor. Only weak signals are measured for eyes in the range where the signal strength drops below this threshold of 0.4.

#146653 - $15.00 USD Received 2 May 2011; revised 15 Jun 2011; accepted 15 Jun 2011; published 17 Jun 2011

The poor performance for eyes with low corneal retardance suggests that we should add a fixed amount of artificial "corneal" birefringence to the RBS system. In terms of Poincaré sphere representation of polarization states, a fixed double-pass wave plate is added that has the effect of shifting the polarization states of the light incident on the retina to the position on the Poincaré sphere where the retinal retardance will have the greatest effect on the size of the generated path of polarization states, and then on the return path will have the effect of shifting the polarization states of the generated path of polarization states back to the position on the Poincaré sphere where the path of polarization states will project maximally onto the S1 axis – yielding the largest retina-derived S_1 signal.

2.3. Validation arrangement: RBS-based eye fixation monitor

An altered version of the monocular RBS-based eye fixation monitor described in Reference 20 was used for model validation purposes. Its RBS system was modified to allow for incorporation of a double-pass retarder at various azimuths, operating in both the incoming and return paths, by means of a custom-made aluminum holder, screwed to the cage cube holding the polarizing beam splitter (PBS) (see Fig. 2). The holder is tilted approximately 10° to reduce specular reflections of light from the flat double-pass surfaces of the wave plate back into the system, which would create much optical noise. The retarder can optionally be attached to the angled holder by means of a rotary mount. The rotary mount is graduated in 2-degree increments, allowing manual rotation of the wave plate's fast axis to various verifiable orientations.

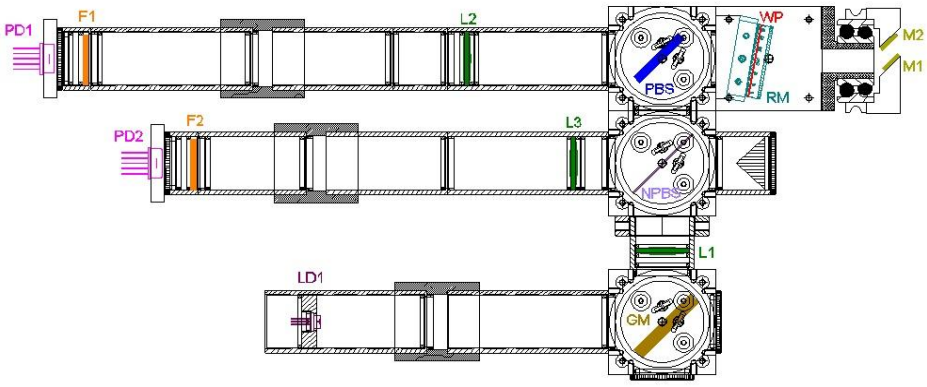

Fig. 2. Top view of opto-mechanical layout of the RBS system of the monocular eye fixation monitor, with added holder for optional inclusion of a wave plate (WP) by means of a rotary mount (RM). A 785 nm laser diode (LD1) produces linearly vertical polarized light, which is deflected by a gold mirror (GM) through a 100 mm f.l. biconvex lens (L1) and a non-polarizing beam splitter (NPBS). The light is then reflected by a polarizing beam splitter (PBS) into a scanning unit, which consists of two plane gold mirrors (M1 and M2). As the mirrors are spun (f = 40 Hz) by a motor (not shown), the stationary beam is converted into a circular scan, pivoting about the center of a stationary 30 mm exit pupil at the subject's eye overfilling the subject's pupil. The scanned circle of light seen by the subject subtends an angle of approximately 3° at the subject's eye (not shown). By the eye's own optics, the beam is focused on the retina, and a portion of this light reflected from the ocular fundus follows the same path back out of the eye. The PBS separates the polarization-altered light into two orthogonal components. The horizontal polarization component is transmitted, passes through a 100 mm f.l. biconvex lens (L2) and a bandpass filter (780 ± 8) nm (F1) with a full width half maximum (FWHM) of (30 ± 8) nm, before finally reaching one of the two photodetectors (PD1). The vertical polarization component is reflected by the polarizing beam splitter (PBS), and part of the vertically polarized light is directed by the NPBS towards the second photodetector (PD2) after passing through another biconvex lens (L3) and bandpass filter (F2) with the same properties. The electronically balanced outputs of the pair of photodetectors are subtracted, yielding the differential polarization signal (S_1 signal).

#146653 - $15.00 USD Received 2 May 2011; revised 15 Jun 2011; accepted 15 Jun 2011; published 17 Jun 2011

2.4. Optimizing foveal fixation detection using wave plates

We needed to find a double-pass wave plate that would statistically optimize foveal fixation detection with the RBS-based eye fixation monitor, preferably uniformly over the population range of corneal retardance and azimuth. With the objective of maximizing RBS signal strength while minimizing the variability of the scan between eyes and among subjects, an algorithm was developed for optimizing both retardance and azimuth (fast axis orientation) of the fixed double-pass wave plate (WP). In the RBS computer model, the wave plate with unknown retardance, δ_{WP}, and azimuth, θ_{WP}, was inserted into Eq. (1):

$$\begin{aligned}\vec{S}_{out} = {} & \mathbf{M}_{WP(out)}(\delta_{WP}, -\theta_{WP}) \cdot \mathbf{M}_{cornea(out)}(CR, -CA) \cdot \mathbf{M}_{retina(out)}(\delta_r, -\theta_r) \\ & \cdot \mathbf{M}_{fundus} \cdot \mathbf{M}_{retina(in)}(\delta_r, \theta_r) \cdot \mathbf{M}_{cornea(in)}(CR, CA) \cdot \mathbf{M}_{WP(in)}(\delta_{WP}, \theta_{WP}) \cdot \vec{S}_{in}.\end{aligned} \tag{6}$$

Since the RBS-based eye fixation monitor, due to its monocular nature, allows measurement of only one eye at a time, the optimization algorithm was applied to only the "right" eye data in the Knighton/Gramatikov data set. A solution to the corneal birefringence problem that works for the right eye will yield a mirror-symmetric solution for the left eye. A mirror-symmetric solution greatly simplifies the mechanical realization in the actual apparatus, in that it requires the wave plate simply to be rotated equal amounts about 90°, depending on whether the right or left eye is examined. For the 150 "right" eyes in the available data set, the double-pass wave plate was computed that would statistically maximize RBS signal strength, while having the greatest independence from the various amounts and orientations of corneal birefringence. Optimization was achieved by varying the properties of the wave plate on a grid ranging from 0° to 180° retardance (0 nm to 393 nm at 785 nm wavelength), and from 0° to 180° azimuth. To minimize processing time, both variables were first stepped through in increments of 10° (i.e. 22 nm for the retardance), sufficient to localize the approximate best range of retardance and azimuth, and then in 1° (2 nm at 785 nm wavelength) steps for the retardance and 2° steps for the azimuth, within this best range. An incremental resolution of 2° seemed reasonable for the azimuth of the WP, considering the 2° graduation of the WP rotation mount incorporated in the experimental validation arrangement. For each incremental step, the mean and standard deviation of the RBS signal strengths (FFT power at 2*f*) of the 150 representative "right" eyes were calculated. The normalized standard deviation, in other words the standard deviation divided by the mean for each retardance/azimuth combination, was then determined, and the minimum of these normalized standard deviations was computed according to the requirement of finding a retardance/azimuth combination that yields maximal signal strength with the least variability across CR and CA. The lowest normalized standard deviation of RBS signal strength for the 150 "right" eyes in the available data set was chosen to identify the best retardance/azimuth combination for the wave plate to add to the monocular eye fixation monitor.

2.5. Method of determining corneal birefringence of studied eyes

Both the corneal retardance and corneal azimuth of our subjects' corneal birefringence had to be known in order to be able to compare the predicted results from the computer model with actual measurements. Individual corneal birefringence was measured with the help of a GDx-VCC instrument (Carl Zeiss Meditec AG, Jena, Germany), available in our institution. The GDx is a commercially available scanning laser polarimeter with an imaging wavelength of 780 nm primarily used for glaucoma diagnosis purposes. The variable corneal compensator version (VCC) of the instrument features two identical wave plates in rotary mounts that allow measurement and individual neutralization of corneal birefringence [14,15]. Given that the examined eye has a normal macula with no disease, the "bow-tie" method can be employed to measure individual corneal birefringence. Corneal birefringence is determined with the magnitude of the VCC set to zero, accomplished by simply rotating both retarders such that their fast axes are perpendicular to each other, in other words with the retarders in the "crossed" position. Macular polarimetry images obtained in this "crossed" position

#146653 - $15.00 USD Received 2 May 2011; revised 15 Jun 2011; accepted 15 Jun 2011; published 17 Jun 2011

demonstrate a non-uniform retardation map with a distinct "bow-tie" pattern centered on the fovea, reflecting the retardation of the cornea superimposed onto the radial retardation distribution of the Henle fiber layer. The eye-specific corneal polarization axis can be determined directly from the orientation of the bow-tie, with the fast axis of corneal birefringence being aligned with the dark arms of the bow-tie, representing macular regions where the Henle fiber retardance subtracts from the corneal retardance. In contrast, the slow axis of corneal birefringence corresponds to the orientation where the bow-tie pattern is brightest, representing macular regions where the Henle fiber retardance adds to the corneal retardance. The magnitude of corneal birefringence (single-pass corneal retardance) is determined by analyzing the retardance profile along a circle around the fovea, with the slow and fast axes of corneal birefringence corresponding to the maximum and minimum values respectively. Corneal retardance can be computed by performing a least-squares fit of the equation

$$\cos\delta_T = \cos\delta_R \cos\delta_C - \sin\delta_R \sin\delta_C \cos 2(\theta_R - \theta_C) \tag{7}$$

to the measured macular retardation profile.

Corneal slow axis (CSA) values obtained with the GDx-VCC (measured nasally downward for each eye, as in [10]), have to be converted to corneal fast axis (CA) values as described above using Eq. (5) to match the corneal parameters in our model.

3. Results

3.1. Finding the optimum double-pass wave plate

As shown in Fig. 3(a) below, there are two local areas of minimal normalized standard deviation. With an incremental resolution of 10° (i.e., 22 nm for the retardance), the optimization algorithm measured an absolute minimum with a wave plate (WP) having a retardance of 60° (131 nm at 785 nm wavelength) and an azimuth of 140°. The algorithm was re-applied, varying the retarder properties on a finer grid covering the area adjacent to the absolute maximum (120° to 160° WP azimuth and 50° to 70° (141 nm to 153 nm) WP retardance), in increments of 1° for the retardance (i.e. 2 nm at 785 nm wavelength) and 2° for the fast axis orientation (see Fig. 3(b)). Maximal RBS signal strength with the least variance

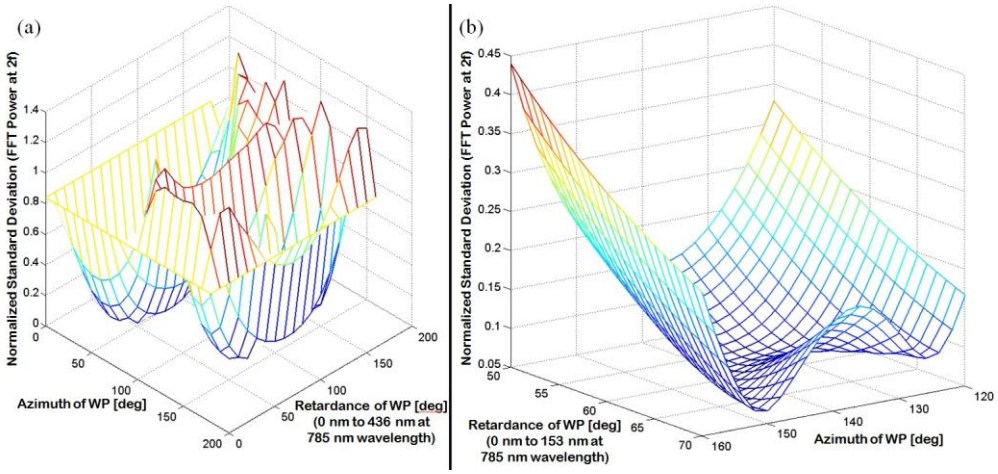

Fig. 3. Normalized standard deviation of RBS signal strengths of the "right" eyes in the Knighton/Gramatikov data set as a function of retardance and azimuth (fast axis orientation) of the double-pass wave plate. (a) Both retarder properties were varied with an incremental resolution of 10° (i.e. 22 nm for the retardance). (b) Retardance and azimuth of the wave plate were varied with an incremental resolution of 1° (i.e. 2 nm at 785 nm wavelength) and 2° respectively, within the best range of minimal normalized standard deviation from (a).

#146653 - $15.00 USD Received 2 May 2011; revised 15 Jun 2011; accepted 15 Jun 2011; published 17 Jun 2011

across the Knighton/Gramatikov range of "right" eye corneal retardances and azimuths was achieved with a 61° wave plate (i.e., a 133 nm retarder at 785 nm wavelength) with fast axis at 144°.

Adding a 61° (133 nm) wave plate to the RBS design, operating on both incoming and returning paths through the eye, theoretically improves foveal fixation detection with the monocular eye fixation monitor. Figure 4(a) shows that with the added wave plate at the fixed orientation of 144°, the RBS signal becomes very large for right eyes with low corneal retardance. RBS signal strength decreases slightly for eyes with high corneal retardance. But compared with the model predications without the wave plate, the signal is practically uniform across the Knighton/Gramatikov range of "right" eye corneal retardances and azimuths in the population (circles). The worse performance at higher values of CR makes little difference, because there was no "right" eye in the Knighton/Gramatikov data with a retardance above 100 nm. The contour plot reveals that none of the representative "right" eyes (circles) falls below the contour of 0.4 (see Fig. 4(b)).

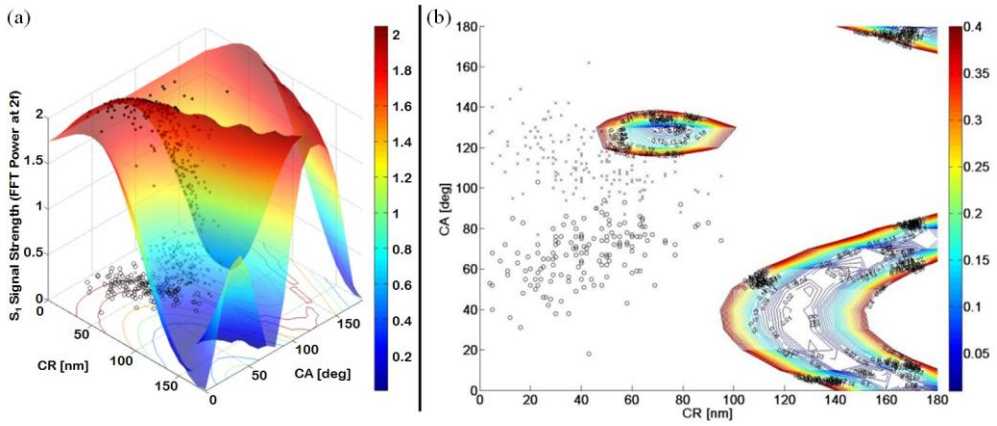

Fig. 4. (a) RBS signal strength at 2*f* (in relative power units) as a function of CR and CA during simulated central fixation with computer model of the RBS design implemented into the monocular eye fixation monitor after adding a double-pass 61° (133 nm) wave plate with fixed azimuth of 144°. (b) Contour plot of (a), with contours plotted only up to a signal strength of 0.4. Eyes that fall within the white regions (where the signal is above the threshold of 0.4) will yield strong enough signals for reliable detection, and eyes in the colored regions will not. Please note the different scales on the color bar. Right eyes (and mirrored left eyes) are indicated as circles and left eyes (and mirrored right eyes) as crosses.

3.2. Verification with human subjects

To compare RBS model predictions with actual measurements, six normal subjects (age 26 - 56) were recruited for the investigations, which were approved by the Johns Hopkins University Institutional Review Board and which adhered to the tenets of the Declaration of Helsinki. Prior to the experiment, the nature and possible consequences of the study were explained, and informed consent was obtained from all subjects.

Four of the six subjects had a refractive error of less than ±2.00 D of sphere, and one subject (2) was measured wearing contact lenses to compensate for 5.00 D of myopia. The monocular eye fixation monitor was designed to function with up to ±2.00 D of refractive error. One subject (3) had astigmatism of 1.50 D (right eye).

Knowing the individual corneal birefringence of the six test subjects is required for predicting their individual results obtained with the monocular RBS system, and thus essential for direct comparison purposes between predicted and measured results. Thus, for all volunteers, individual corneal retardance and azimuth were measured with the GDx device as described above. Two macular polarimetry images were acquired for each subject, and the mean corneal retardance and azimuth were used for the analysis, as presented in Table 1.

#146653 - $15.00 USD Received 2 May 2011; revised 15 Jun 2011; accepted 15 Jun 2011; published 17 Jun 2011

Table 1. Measured corneal retardance (CR) and corneal azimuth (CA) for studied right eyes

	Right Eye	
Subject	CR [nm]	CA [deg]
1	33.7	77
2	27.3	50
3	22.0	74
4	29.0	58
5	37.0	70
6	27.0	77

3.3. Model predictions for studied eyes

With both corneal retardance and corneal azimuth of our subjects known, the performance of the monocular eye fixation monitor (in terms of strength of the foveal fixation signal) can be predicted for each right eye. To determine the predicted foveal fixation signal strength obtained with the eye fixation monitor, the measured values of corneal retardance and azimuth from Table 1, for each subject, were inserted into the RBS model, which calculated the S_1 signal strength during simulated central fixation with the model of the monocular eye fixation monitor, both with and without the added 61° (133 nm) wave plate oriented at 144°. The RBS model predicts that foveal fixation detection is greatly improved for each of the 6 studied right eyes after adding the fixed amount of 61° (133 nm) retardance (see Table 2).

As another comparison measure, we also calculated the fast axis orientation for the given 61° (133 nm) wave plate that would statistically maximize RBS signal strength for each subject, using that subject's measured combinations of CR and CA. Individual optimization was achieved by varying the azimuth of the wave plate from 0° to 180° in increments of 2°, for the given retardance of 61° (133 nm). For each azimuth, the FFT power at $2f$ was computed, and the azimuth with the highest number, that is maximal signal strength, was chosen to be the best orientation for the specific right eye. The results are given in Table 2.

Table 2. Predicted RBS signal strength in relative power units during simulated central fixation with computer model of monocular eye fixation monitor for studied right eyes[a]

	Predicted FFT Power at $2f$		Opt. WPA
Subject	No WP	With WP	[deg]
1	0.11	2.03	62
2	0.35	2.12	70
3	0.07	1.98	64
4	0.33	2.12	68
5	0.27	2.11	66
6	0.07	1.98	64

[a]Obtained both without (No WP) and with optimized 61° (133 nm) wave plate (With WP), and individual optimized fast axis orientation for the given 61° (133 nm) wave plate (Opt. WPA) that yields maximal RBS signal strength during simulated foveal fixation for each studied right eye.

These results show that for our six test subjects a fast axis orientation of approximately 66° (average of Opt. WPA in Table 2) would theoretically be better suited for the right eye measurement with the monocular eye fixation monitor, which lies within the second suggested local area of minimal normalized standard deviation (see Fig. 3(a)). Recall that the optimization algorithm calculated two local areas of minimal normalized standard deviation for the monocular RBS design, with the absolute minimum occurring at 144°, which was optimized for Knighton and Gramatikov's population range of “right” eye corneal birefringence (total of 150 “right” eyes). The modeling results with the wave plate oriented at 66° are shown in Fig. 5(a) in form of the familiar 3D-plot. As can be seen, with the 61° (133 nm) wave plate oriented at 66°, the RBS signal becomes very large and uniform for right eyes with low corneal retardance, but falls off with higher values of CR. Thus, considering the entire population range of right eye corneal birefringence (with the Knighton/Gramatikov data as reference), RBS signal strength is less uniform with the wave plate oriented at 66° than at 144° (see Fig. 4(a)). However, a fixed azimuth of 66° greatly enhances foveal fixation

#146653 - $15.00 USD Received 2 May 2011; revised 15 Jun 2011; accepted 15 Jun 2011; published 17 Jun 2011

detection for the right eyes of our test subjects, whose highest value of CR was only 37 nm (subject 5).

Figure 5(b) details, for one subject (#1), the predicted RBS signal strength at 2*f* as a function of fast axis orientation of the 61° (133 nm) wave plate. The individually-applied optimization algorithm in the computer model predicted an absolute maximum in FFT power at 2*f* with the fast axis oriented at 62°.

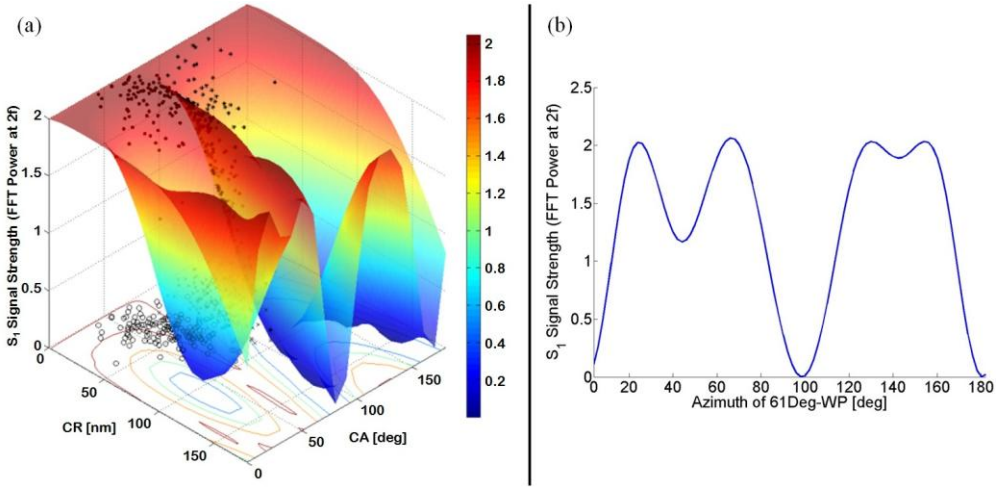

Fig. 5. (a) RBS signal strength at 2*f* (in relative power units) as a function of CR and CA during simulated central fixation with computer model of the monocular RBS-based eye fixation monitor after adding a double-pass 61° (133 nm) wave plate with fixed azimuth of 66°. (b) RBS signal strength at 2*f* (in relative power units) plotted as a function of fast axis orientation of the added 61° (133 nm) wave plate, for a given pair of right eye corneal retardance and azimuth (CR = 33.7 nm, CA = 77°) during simulated central fixation with computer model of the monocular RBS-based eye fixation monitor.

3.4. Measured data from studied eyes

To compare model predictions with experimental data, the right eye of the six subjects was measured with the validation arrangement described in 2.3. Subjects were seated in front of RBS-based eye fixation monitor and were instructed to look into the active eyepiece with the right eye, while placing their forehead against the faceplate to simplify head positioning [20]. Room lights were turned off to enhance pupil dilation, and thus to allow more light to enter the eye. Subjects were asked to fixate centrally on the blinking visible fixation light in the center of the faint 785 nm scanning circle and press the trigger on a handheld pushbutton to initiate data acquisition, maintaining fixation for about half a second until acquisition was complete. This procedure was performed both without and with a wave plate (AX27341, Anchor Optics; Barrington, NJ) added to the double-pass system, which we measured as having a retardance of 61° (133 nm) at our operating wavelength of 785 nm, using the principle of the "crossed" polarizer method [31].

Measurements in the wave plate mode were first obtained with the retarder oriented at the position optimized for Knighton and Gramatikov's population range of corneal birefringence, i.e., at 144°. Next, data were acquired for each subject with the wave plate rotated to the individual optimized fast axis orientation from Table 2. The foveal fixation signal strength measured in each setting is presented in Table 3 (FFT power of the fixation reading, at twice the scanning frequency).

In addition, for one subject (#1), the 61° (133 nm) wave plate was manually rotated through 180° in incremental steps of 10°, and the strength of the foveal fixation signal at each incremental step was measured to experimentally determine the fast axis orientation that

#146653 - $15.00 USD Received 2 May 2011; revised 15 Jun 2011; accepted 15 Jun 2011; published 17 Jun 2011

Table 3. Measured RBS signal strength of right eyes of the subjects (in relative power units)[a]

	Measured FFT Power at 2*f* (relative units)		
Subject	No WP	With WP	With WP at Opt. WPA
1	0.25	0.30	1.15
2	0.24	0.60	0.46
3	0.03	0.04	0.09
4	0.35	0.27	0.98
5	0.14	0.17	0.48
6	0.18	0.35	0.85

[a]Measured during central fixation with the monocular RBS-based eye fixation monitor, both without (No WP) and with the 61° (133 nm) wave plate. The retarder was oriented at 144° first (With WP), before it was rotated to the predicted optimal position for each subject (With WP at Opt. WPA).

yielded maximal FFT power at 2*f*. With an incremental resolution of 10°, maximal signal strength was measured with the 61° (133 nm) wave plate oriented at 60°. Adjacent to 60°, the retarder was then rotated in 2° steps to find the absolute maximum. The maximal FFT power at 2*f* was measured with the wave plate oriented at azimuth 64°.

4. Discussion and conclusion

The measurement results show that for all subjects, except one (#4), the strength of the RBS signal during central fixation increased after adding the 61° (133 nm) wave plate oriented at 144° to the optical system, as predicted with the RBS computer model. Note that subject #4 already yielded a remarkably high foveal fixation signal without the wave plate, compared with the signal strength measured without the wave plate for the other tested right eyes, even higher than the foveal signal for subjects 1, 3, and 5 measured after the 61° (133 nm) wave plate had been added to the optical system.

In accordance with RBS model predictions, foveal signal strength is even further increased for the test subjects (except subject #2) with the wave plate oriented at the individually optimized azimuth. This confirms the hypothesis that for our small group of tested subjects, a fast axis orientation of about 66° is better suited for the right eye measurement with the monocular eye fixation monitor, significantly enhancing foveal fixation detection.

For subject #3, RBS signal strength is in general low, which might be explained by the astigmatism present in the subject's right eye, causing less useful light to return to the detector after the double-pass through the ocular system. The eye serves as an efficient retro-reflector only when the retina and the source of light are situated in conjugate planes, in other words with the eye being properly focused on the light source. This assumption is included in the RBS computer model, but it is certainly not valid for the astigmatic right eye of subject #3.

There are possible limitations of the RBS computer model, and possible errors in the assumptions used in its development, that may be contributing to deviations between measurements and model predictions. First, even though polymer retarders, such as the 61° (133 nm) wave plate used, are much less sensitive to changes in retardance with changes in the angle of incidence (if tilted about its fast or slow axis), the 10° tilt, minimizing specular back reflections, could have introduced significant errors with the fast axis rotated to its optimized azimuth. Also, the tilt changes the retarder's fast axis azimuth slightly with respect to the beam reference system. In other words, the actual fast axis orientation will differ from the manually adjusted azimuth on the rotary mount, more precisely it will be shifted towards lower angles. This explains the observed deviation of 2° between measured and predicted fast axis azimuth that yields maximal foveal signal strength for subject #1. The theoretically predicted value, 62°, was 2° less than the measured result, 64°.

Second, different head positioning during the assessment with the GDx instrument and the monocular eye fixation monitor could cause differences in measured and actually present corneal birefringence during data acquisition with the monocular RBS-based eye fixation monitor. In fact, measurements with the GDx are limited to the central cornea, whereas with

#146653 - $15.00 USD Received 2 May 2011; revised 15 Jun 2011; accepted 15 Jun 2011; published 17 Jun 2011

the large exit pupil used in retinal birefringence scanning, to allow relative freedom of the subject's head, the entire cornea overlying the pupil is used. Thus non-uniformity of corneal birefringence across the pupil of real eyes can be a major confounding factor potentially resulting in inconsistent agreement between model predictions and measurement results. Such irregularity is undoubtedly present with the large pupils induced during the assessment with the monocular RBS-based eye fixation monitor by turning off room lights to allow more light to enter the eye.

Another potential source of error includes the assumption that the fundus acts as an ideal retro-reflecting surface, modeled by the Müller matrix of an ideal mirror. In real eyes only a small portion of the light incident on the retina is reflected (about 1/10,000 to 1/1000 of the light is reflected) [1], which varies across individuals.

Despite the potential sources of errors, the preliminary validation experiments with human subjects using the monocular RBS-based eye fixation monitor showed that the RBS computer model is capable of assessing the influence of varying corneal birefringence on the strength of the differential RBS signal during foveal fixation. The data obtained confirmed the model's ability to predict an appropriate double-pass wave plate, which, when added to the optical system, improves RBS signal strength during central fixation.

In conclusion, the RBS computer program described in this paper allows assessment of the effect of varying corneal birefringence on the strength of the RBS signals. It also provides a means of optimizing RBS using wave plates and other optical components. "Wave-plate-enhanced" RBS enhances recognition of foveal fixation by minimizing the deleterious effects of corneal birefringence. We are currently completing a binocular RBS system incorporating spinning and fixed wave plates [32].

Acknowledgments

This work was supported in part by gifts from Robert and Maureen Feduniak, Dewey and Janet Gargiulo, David and Helen Leighton, Richard and Victoria Baks, Robert and Diane Levy, and by awards from Research to Prevent Blindness (DG), the Hartwell Foundation (BG), and the Knights Templar Eye Foundation (KI). The authors thank Robert W. Knighton and Xiang-Run Huang for the corneal birefringence data from 70 human subjects, and Carl Zeiss Meditec for providing assistance with the GDx-VCC manuals and a software update.

#146653 - $15.00 USD Received 2 May 2011; revised 15 Jun 2011; accepted 15 Jun 2011; published 17 Jun 2011